Palaeogeography, Palaeoclimatology, Palaeoecology 502 (2018) 74–85

Contents lists available at ScienceDirect

Palaeogeography, Palaeoclimatology, Palaeoecology

journal homepage: www.elsevier.com/locate/palaeo

Middle to late Holocene delta plain evolution of the Kimotsuki lowland, Kyushu (southern Japan)

Yuji Ishii[1]

Department of Geography, Graduate School of Environmental Studies, Nagoya University, Furocho, Chikusa-ku, Nagoya, Aichi 464-8601, Japan

ARTICLE INFO

Keywords:
Peat
Climate change
East Asian summer monsoon

ABSTRACT

The evolution of delta plains and coastal floodplains is commonly believed to be influenced by sea-level and climate changes. However, regional climate change influences on the evolution of delta plains and floodplains are poorly understood compared with responses to rapid sea-level rise since the last deglaciation. This study investigated the Kimotsuki lowland delta plain evolution (Kyusyu, southern Japan), including allogenic controls, based on 28 auger cores and 28 radiocarbon ages. Large-scale crevasse splay deposition occurred at 7000–6000 cal yr BP in response to sea-level rise or increased sediment supply following a volcanic eruption. Afterwards, widespread peat was formed in the absence of substantial fluvial sedimentation. Decreased precipitation from a weakened East Asian summer monsoon may have dried the peatlands around 4000 cal yr BP. With increasing precipitation and storminess around 2000 cal yr BP, peat formation resumed at areas further from the Kimotsuki River, while increased overbank flows deposited organic-rich mud near the river. These changes may reflect an increased frequency of La Niña events and higher ocean surface temperatures of the Kuroshio extension. The increased storminess around 2000 cal yr BP may have produced similar influences on delta plain and coastal floodplain evolution across the East Asia region. The results of this study suggest that regional climate change in the late Holocene has a potential to control the evolution of coastal floodplains and delta plains.

1. Introduction

Allogenic controls on fine-grained coastal floodplains and delta plains, such as climate change, sea-level fluctuations, and neotectonics are well documented across several disciplines, including geomorphology, geology, and archaeology (Aslan and Autin, 1999; Aslan and Blum, 1999; Blum and Törnqvist, 2000; Stouthamer and Berendsen, 2001, 2007; Pennington et al., 2016). Climate change during the middle to late Holocene was driven by declining summer insolation in the Northern Hemisphere (Wanner et al., 2008; Marcott et al., 2013). Some recent studies suggest this substantial climate change influenced the evolution of coastal floodplains and delta plains. The rarity of large-scale crevassing and slower aggradation in the Nile delta after 6000–5000 cal yr BP (Marriner et al., 2012a, 2012b; Pennington et al., 2017) are associated with decreased African monsoon precipitation (Shanahan et al., 2015), although decreased sea-level rise may have contributed more to the slower aggradation (Pennington et al., 2017). Similarly, decreased precipitation from a weakened EASM reduced fluvial activity and led to near-cessation of overbank deposition followed by widespread peat initiation at 5600–5000 and 4100–3600 cal yr BP in the Ishikari and Shiribeshi-Toshibetsu River lowland, northern Japan (Ishii et al., 2016; Ishii, 2017a). These studies suggest that climate change in the middle to late Holocene had a substantial influence on the evolution of coastal floodplains and delta plains.

In contrast, the impact of regional climate change on the floodplain evolution in the late Holocene is not well understood because the magnitude of regional climate change generally seems to be small. In the EASM region, precipitation was reduced throughout the late Holocene due to the reduced summer insolation in the Northern Hemisphere (Dykoski et al., 2005). Meanwhile, a large increase in sediment discharge from man-made deforestation occurred in many Asian large rivers (Saito et al., 2001; Tanabe et al., 2006), and its impact on the floodplain evolution may be substantial. Previous studies inferred that the active fluvial deposition was highly influenced by increased sediment discharge from man-made deforestation (Kawase, 1998; Hasada, 2015; Itoh et al., 2017). However, the active overbank sedimentation may reflect the activity of El Niño-Southern Oscillation (ENSO) because it is related to the magnitude and frequency of tropical storms and typhoons in the East Asia region (e.g. Camargo et al., 2007).

E-mail address: ishii.yuuji@f.mbox.nagoya-u.ac.jp.
[1] Research Fellow of the Japan Society for the Promotion of Science, Japan.

https://doi.org/10.1016/j.palaeo.2018.04.025
Received 31 October 2017; Received in revised form 26 April 2018; Accepted 27 April 2018
Available online 01 May 2018
0031-0182/ © 2018 Elsevier B.V. All rights reserved.

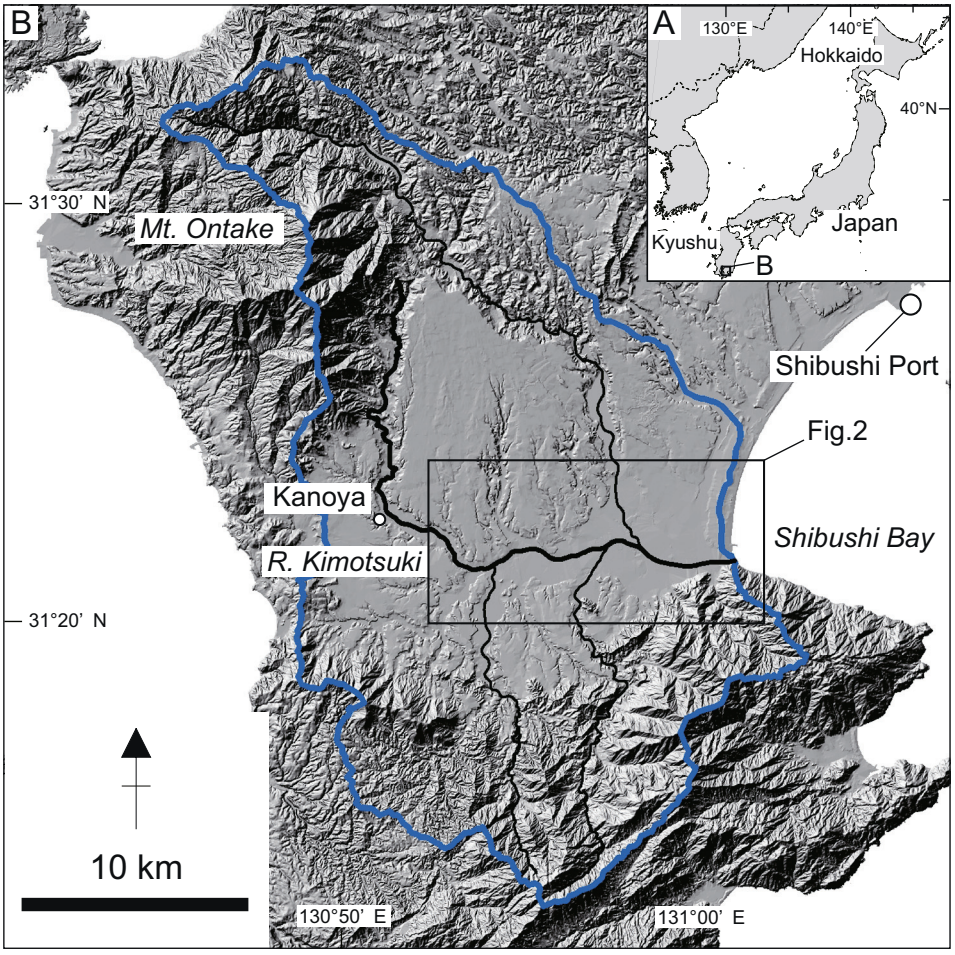

Fig. 1. Map showing the study area. A. Kimotsuki River lowland location. B. Shaded-relief map of the Kimotsuki River basin and surrounding area. The blue line indicates the watershed boundary. (For interpretation of the references to color in this figure legend, the reader is referred to the web version of this article.)

Zhu et al. (2017) recently indicated that the magnitude and frequency of floods increased after 2000 cal yr BP in central China possibly in response to enhanced ENSO activity. More research is needed to better understand the susceptibility of floodplains to the regional climate change in the late Holocene.

A detailed floodplain chronology is necessary to understand fluvial responses to centennial-scale changes in regional climate. The presence of widespread peat enables a reconstruction of detailed floodplain chronology because peat includes abundant plant and wood fragments suitable for radiocarbon dating and widespread peat initiation or cessation reflects a major change in sedimentary environment (Ishii et al., 2016; Ishii, 2017a). While widespread peat is relatively common on delta plains and coastal floodplains in the northern part of Honshu and Hokkaido, it rarely occurs to the south (Sakaguchi, 1974). Although the conditions for a dearth of peat in central and southern Japan are not completely clear, higher temperatures in coastal areas may inhibit peat formation (Yabe, 1989; Tomita, 2010). One exception is the Kimotsuki River delta plain in southern Japan (Kyushu, Fig. 1), where widespread peat layers develop up to 4 m thick. Abundant spring water from the surrounding plateau appears to promote peat formation (Sakaguchi, 1960; Arizono, 1985). This indicates that the peat formation is susceptible to changes in the amount of precipitation and thus a good indicator for climate change, while it is also affected by fluvial deposition near the river due to enhanced storminess. Therefore, climate change and fluvial activity may influence the delta plain evolution in a different way, which allows a reliable comparison of fluvial activity with climate change.

Peat is absent near the Kimotsuki River and thickens toward the southern edge of the lowland (Sakaguchi, 1960). A radiocarbon age of 6600–6200 cal yr BP was obtained from the base of the peat (Nagasako et al., 1999). A mud layer possibly formed under the influence of climate change and/or human activities overlies the widespread peat (Sakaguchi, 1979; Nagasako et al., 1999). However, the stratigraphy and chronology of the delta plain have not been studied in detail. The purpose of this study is to investigate the evolution of the Kimotsuki River delta plain based on the radiocarbon ages from 28 auger cores and evaluate the influences of EASM and ENSO on the delta plain evolution. A special focus is on the influence of climate change on the increased fluvial activity in the late Holocene.

2. Regional setting

The Kimotsuki River headwaters originate from Mt. Ontake (1182 m elevation) and flow south through the Shirasu Plateau, which was formed by the eruptions from the Aira Caldera around 30,000 cal yr BP (Smith et al., 2013) and is mostly composed of unwelded pyroclastic flow deposits of high permeability (Fig. 1). The river has a catchment area of 485 km^2 and length of 34 km (Kyushu Regional Development Bureau, 2012). The channel gradient is about 0.1% near the confluence with the Aira River and 0.038% at the mouth (Kyushu Regional Development Bureau, 2012). The mean tidal range and wave height at Shibushi Port (Fig. 1) (2010–2014) are 1.11 and 0.42 m, respectively. The tidal influence extends about 6 km upstream of the river mouth.

Mean annual precipitation at Kanoya (Fig. 1) is about 2400 mm (1981–2010), where roughly 70% of the precipitation falls during the EASM season (May–October). The quasi-stationary Baiu and Akisame

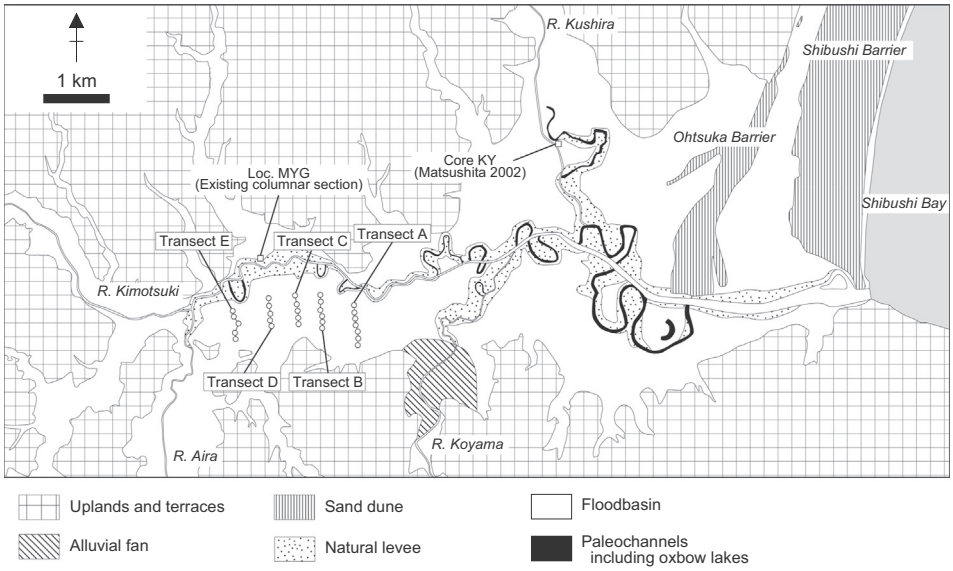

Fig. 2. Landform classification map of the study area showing borehole locations sampled in this study and the core location KY collected by Matsushita (2002) and MYG provided by Kimotsuki town.

rainbands are prominent features of the EASM region, where the Baiu rainband moves slowly northward from early June to August. This northward migration produces heavy precipitation in the region from middle to late June. Mean annual peak flow near the river mouth is 900 m^3/s (1981–2010), often occurring from June to August in association with the Baiu rainband and typhoons.

Natural levees develop along the Kimotsuki River downstream from the confluence with the Aira River (Fig. 2). Paleochannels are only found near the present channel with no apparent avulsions. Typical 19th century cropping systems used in this area suggest the floodbasin was naturally inundated, likely recharged by spring water from the Shirasu Plateau (Arizono, 1985). Peat layers found near the surface of the delta plain (Sakaguchi, 1960; Nagasako et al., 1999) likely began developing at 6500–5500 cal yr BP, based on the basal age of the peat (Nagasako et al., 1999).

The core lithology and relative density of the sediments (N values) at borehole MYG (Fig. 2), provided by Kimotsuki town, show one view of the paleovalley fills stratigraphy (Fig. 3). The paleovalley fills in Japan can be commonly divided into five lithofacies, in ascending order: Basal Gravels, Lower Sand, Middle Mud, Upper Sand, and Terrestrial Sand and Mud (Iseki, 1962; Hori et al., 2011). Basal Gravels are braided river system deposits typically found at the bottom of Japanese paleovalleys. Lower Sand was commonly formed during the last transgression and deposited in fluvial and estuarine environments. The mud with low N values is correlated to Middle Mud and closely corresponds to prodelta deposits in a bay or lagoon. Upper Sand generally overlies Middle Mud and is correlated to delta front deposits. Terrestrial Sand and Mud are mostly fluvial and organic deposits, and this study focuses on this uppermost strata.

Three series of barriers developed along the Kimotsuki lowland coast (Nagasako et al., 1999): Ohtsuka and Shibushi Barriers (Fig. 2), and Yokose Barrier (north of this area). The Ikeda pumice fall (Ik-P, around 6400 cal yr BP; Moriwaki et al., 2016) occurs near the top of the Ohtsuka Barrier around 2–4 m in elevation, indicating that the barrier was above sea level at the time of deposition (Nagasako et al., 1999). The fluvial environment at site KY (Fig. 2), located landward of the Ohtsuka Barrier, established between around 6400 and 4600 cal yr BP (Matsushita, 2002). Nagasako et al. (1999) speculated that the widespread peat is associated with barrier formation based on the similar ages of the emergence of Ohtsuka Barrier and a basal age of peat.

Sea-level fluctuations during the Holocene have not been reconstructed for the region. However, the relative sea-level generally

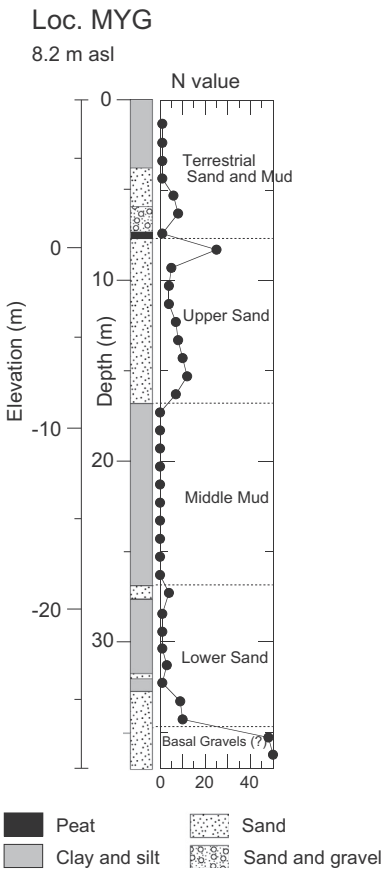

Fig. 3. Columnar section MYG showing one view of the Kimotsuki lowland paleovalley fills provided by Kimotsuki town. The columnar section was made by geotechnical engineers when borehole investigation was conducted at a construction site.

stabilized or slightly fell after 6000–4000 cal yr BP in embayments in Japan due to crustal uplift associated with hydro-isostatic effects (Nakada et al., 1991; Yokoyama et al., 2012; Okuno et al., 2014). The geophysical modeling by Okuno et al. (2014) suggests that sea level around 6000 cal yr BP was roughly 0–2 m higher than today. This is

consistent with the presence of peat at borehole MYG (0.9–0.6 m asl, Fig. 2) and the emergence of the delta plain at a sea level near or slightly higher than the present mean sea level.

Tephra layers are found in paleovalley fills of the Kimotsuki lowland: Sakurajima-Takatoge 3 (Sz-Tk3, around 10,600 cal yr BP), Kikai-Akahoya (K-Ah, 7300–7150 cal yr BP), Ikeda pumice fall (Ik-P, around 6400 cal yr BP), Sakurajima-Takatoge 2 (Sz-Tk2, around 5000 cal yr BP), Kirishima-Miike (Kr-M, around 4600 cal yr BP), Kaimondake 9c (Km9c, around 1900 cal yr BP), and Kaimondake 12a (Km12a, 874 CE) (Nagasako et al., 1999; Matsushita, 2002; Moriwaki et al., 2016). The K-Ah tephra includes extensive Koya pyroclastic flow deposits as well as K-Ah ash fall, and those deposits are also found on the Shirasu Plateau around the Kimotsuki lowland (Matsushita, 2002). The thickness of the Koya pyroclastic flow deposits reaches approximately 40 cm in the southern part of the catchment and 10 cm on the north side of the lowland on the Shirasu Plateau (Machida and Arai, 1978; Fujiwara and Suzuki-Kamata, 2013). Pollen analysis of sediment from borehole KY (Fig. 2) indicates the Kikai-Akahoya eruption destroyed vegetation in the study area that recovered after several centuries (Matsushita, 2002). The Ik-P may have similarly impacted vegetation as the tephra thickness reached a maximum of 1 m in the southern part of the catchment (Kawabe and Sakaguchi, 2005).

3. Material and methods

A field investigation was conducted in September 2016, where 28 sediment cores up to 4.5 m long were collected with a hand auger. Five transects were established roughly perpendicular to river flow (Transects A to E) and cores collected along each transect were numbered with the corresponding prefix 'A' to 'E' (Figs. 2 and 4). Cores along each transect were numbered in ascending order with distance from the river (Fig. 4). Sediment cores were collected at intervals of 70–140 m along each transect. Sediments were described and photographed in the field and subsampled at 5 cm for loss on ignition (LOI) analysis. Plant fragments were also picked out for radiocarbon dating. A global navigation satellite system was used to determine the surface elevation at boreholes. The raw data were collected in the static method and were post-processed in the office. The elevation was measured relative to Tokyo Peil datum (TP; mean sea level of Tokyo Bay).

LOI of sediment was determined at 10 cm intervals to distinguish peat from clastic deposits. Sediment was dried at 80 °C for 48 h and 0.5–3.0 g (dry weight) subsamples were heated in an electric muffle furnace at 750 °C for 1 h. Sediment was classified as peat for LOI values > 20%, organic-rich mud for LOI values of 10–20%, and mud for LOI values of < 10% (Ishii et al., 2016; Ishii, 2017a). This classification is reasonable because LOI reflects significant changes in clastic input when LOI values are < 20%, while LOI reflects slight changes in clastic input when LOI values are > 20% (Ishii et al., 2016).

Radiocarbon ages were obtained from plant and wood fragments by accelerator mass spectrometry (Table 1). The samples were cleaned in an ultrasonic bath with distilled water and processed by the standard acid-alkali-acid treatment. The pretreated samples were submitted to DirectAMS (Bothell, Washington, USA). The radiocarbon ages were calibrated with the OxCal 4.2 program (Bronk Ramsey, 2009) based on atmospheric data from Reimer et al. (2013). An age–depth model was constructed based on the median probability of the calibrated radiocarbon ages and a tephra layer (Kr-M). Compaction effects were not considered in the age–depth model.

Aerial photographs (1:30000, taken in 1947 by the U.S. Army) were used to produce the landform classification map of the study area (Fig. 2). Peatlands could not be identified from the photographs due to coverage by overbank deposits (> 0.5–1 m thick) and croplands.

4. Results

4.1. Sedimentary facies and interpretation

Very fine to very coarse sands are typically found at or near the base of the cores and are overlain by peat, mud, and organic-rich mud (Fig. 4). Although a few tephra layers were found in some cores, only Kr-M could be positively identified (Fig. 4). Detailed descriptions and interpretations of the sediments are given below, and stratigraphy in the next section.

A light brown to reddish brown tephra layer 1–5 cm thick was found at 1–2 m depth in most cores. The tephra is generally composed of fine well-sorted sands and is reliably correlated to Kr-M, clearly distinguished by color from other tephra layers in the study area (Sakaguchi, 1960; Nagasako et al., 1999).

One or two black to dark purple tephra layers < 5 cm thick were also found above Kr-M at some locations. The volcaniclastic sediments are often mixed with mud, which may indicate that the tephra layers were bioturbated or reworked. Nagasako et al. (1999) reported two tephra layers with similar characteristics above Kr-M and inferred their correlation to Km9c and Km12a, although the criteria for these correlations were not provided. These tephra layers were not used to construct a chronology in this study because their identification is uncertain, in part due to potential bioturbation or reworking.

Peat found in the cores is black and composed of basal sheaths, rhizomes, and herbaceous roots. The organic components are usually not well-preserved, suggesting some decomposition. The LOI values are generally < 50–70%. An upward decrease in peat LOI values is common around the Kr-M (Fig. 4). Peat forms in floodbasins where negligible overbank sedimentation occurs and high water levels are suitable for wetland plants (Törnqvist, 1994; Bohacs and Suter, 1997; Ishii et al., 2016).

Mud and organic-rich mud found in the cores are generally dark grey to black with occasional grey to bluish grey mud, < 5 cm thick. Plant fragments are occasionally found in the mud and organic-rich mud, and the fragments sometimes extend vertically for a few to several decimeters. Muddy deposits with occasional plant fragments are considered floodbasin deposits (e.g. Aslan and Autin, 1999).

Sands at or near the base of the cores often include granule- to pebble-size pumice and plant fragments (Fig. 4). The basal sand layer generally has a sharp contact with the overlying deposits. There are two sand layers at sites C2 and C3, and an erosional contact occurs between the upper sand and underlying deposits at around 2.5 m depth. The sand layer at site C5 also has a sharp contact with the underlying mud. In contrast, the sand layer at sites E4 and E5 shows a gradual coarsening-upward near its base. Nagasako et al. (1999) speculated that these are bay-head delta deposits. However, the abundance of plant fragments and absence of shell fragments suggest fluvial deposition. Floodplain sands can be deposited as natural levees or crevasse splays (Smith et al., 1989; Toonen et al., 2016). Further interpretation using stratigraphy is described in the next section.

A medium to coarse sand layer was found in the core near the surface at borehole E2. The auger could not penetrate deeper than 1.0 m, likely due to hard gravels. The thick sand layer near the surface of core E2 may be deposition from a small tributary at this location.

4.2. Stratigraphy

Fig. 5 shows the borehole lithologic logs arranged by elevation to better correlate the stratigraphy of the delta plain deposits. Peat is generally rare or thin above the Kr-M, and organic-rich mud dominates the upper part of the delta plain deposits. The thickness of the peat between Kr-M and the basal sand layer is generally about 1 m with the exception of thin peat at borehole B1 and the absence of peat at borehole A1, likely due to their proximity to the Kimotsuki River. Above Kr-M, peat thicknesses of 0.5–1.5 m were found at boreholes A5–A7 and

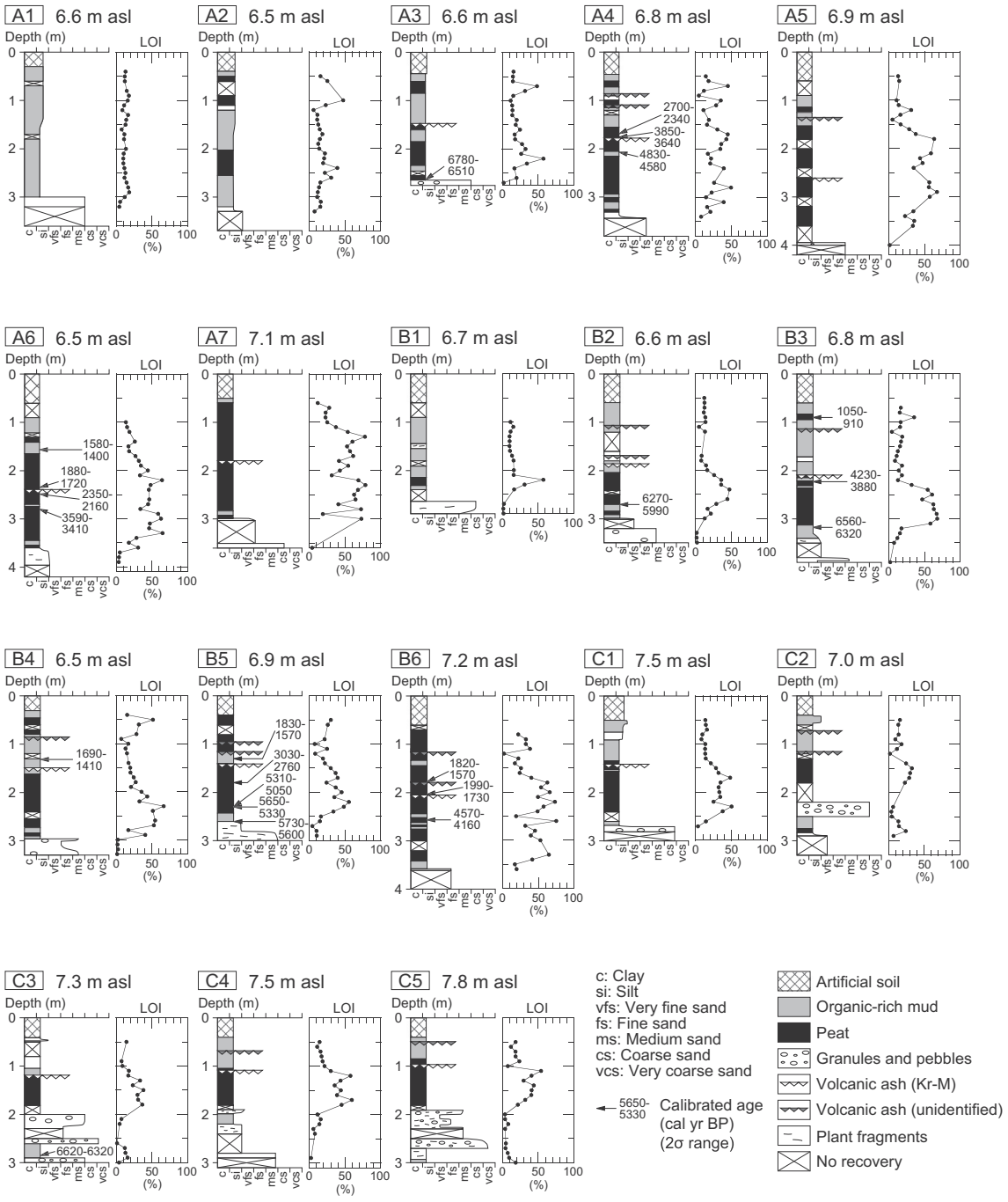

Fig. 4. Columnar sections (borehole lithologic descriptions) and corresponding LOI values for the auger cores collected in this study.

B4–B6, which are further from the river.

In transects A, B, and E, organic-rich mud above Kr-M thins toward the Shirasu Plateau (Fig. 5). Although the thickness of the organic-rich mud above Kr-M is similar along transect C, it does thin slightly toward the Shirasu Plateau. Transect D does not follow this general trend, and organic-rich mud is notable at boreholes D3 and D5.

The top elevation of the basal sands is usually within 1 m along each transect. The sands appear to form a relatively flat topography with a low gradient moving downstream from Transect E to Transect A (Fig. 5). Such flat extensive sand surfaces are often formed by large-scale crevasse splays (Smith et al., 1989; Slingerland and Smith, 2004; Pennington et al., 2016). The top of sand layers in transect C is higher than basal sands along transect D (Fig. 5). These higher elevation sands in transect C may have been deposited by a small-scale crevasse, and the lower sand layers may be correlated to sands at or near the bottom of cores in the other transects.

4.3. Radiocarbon ages

Five radiocarbon ages were obtained near the top of the basal sands at boreholes A3, B2, B3, B5, and D4 (Fig. 5). The ages range from 7000 to 5500 cal yr BP and are consistent with the basal age of peat (6600–6200 cal yr BP) reported by Nagasako et al. (1999) (Fig. 5). In contrast, the base of the peat at borehole D2 had an age of 3830–3510 cal yr BP (Fig. 5), much younger than anticipated considering the depositional age of Kr-M described later. This sample may have been contaminated with the overlying sediments during hand augering or roots may have penetrated down to the sampled area.

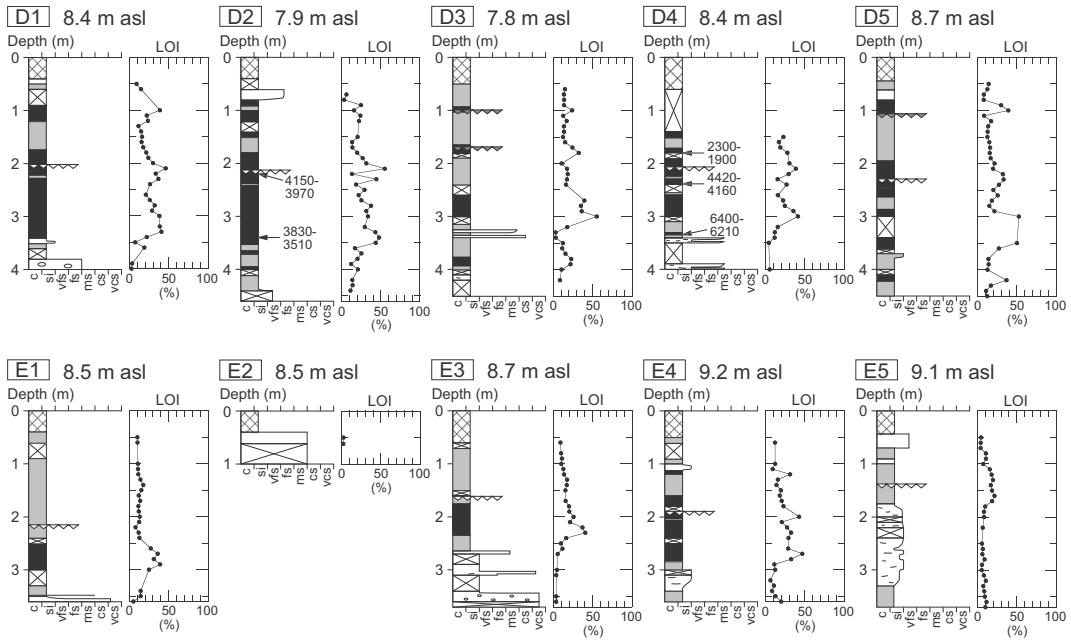

Fig. 4. (*continued*)

The depositional age of Kr-M was estimated from radiocarbon dating of plant fragments within 0.1 m of the Kr-M at boreholes A4, B3, and D2 (Fig. 5). The radiocarbon dating indicates the Kr-M was deposited before 3850–3640 cal yr BP at borehole A4 and after 4200–3900 cal yr BP at boreholes B3 and D2, and the average of these values is about 4000 cal yr BP. Radiocarbon ages of sediment sampled 0.45–0.2 m below the Kr-M at boreholes A4, B6, and D4 are 4800–4200 cal yr BP, which also indicates Kr-M was deposited after 4200 cal yr BP. Collectively, the radiocarbon ages suggest that the Kr-M was deposited roughly 4000 cal yr BP. The age is somewhat younger than those reported by Okuno (2001) for bulk peat 0.1–0.2 m above and below the Kr-M: 4500–4400 and 4900–4700 cal yr BP. The older estimated Kr-M ages by Okuno (2001) may be due to the sampling technique, in which bulk sediments are often contaminated with old carbon and yield an older age (e.g. Grimm et al., 2009). In contrast, much younger Kr-M ages were estimated from plant fragments obtained within 0.1 m of Kr-M at boreholes A6, B5, and B6, with radiocarbon ages of 2400–1500 cal yr BP (Fig. 5). Similar young ages were estimated from sediments 0.3 m below the Kr-M at boreholes A6 and B5. These younger ages may have resulted from the downward penetration of roots. Deposition of organic-rich muds above the Kr-M was also estimated using radiocarbon dating. At boreholes A6, B4, and D4, organic-

Table 1
Radiocarbon ages from the Kimotsuki lowland deposits.

Sample code	Depth (m)	Elevation (m)	Dated material	^{14}C age (yr BP)	Error (1σ)	Calibrated age (cal yr BP) (2σ range)	Median probability (cal yr BP)	Laboratory code
A3-270	2.7	3.9	Wood fragment	5850	55	6790–6510	6670	D-AMS-019971
A4-170	1.7	5.1	Plant fragment	2400	45	2700–2340	2440	D-AMS-022770
A4-178	1.8	5.0	Plant fragment	3485	35	3850–3640	3760	D-AMS-022771
A4-205	2.1	4.7	Plant fragment	4150	55	4830–4530	4690	D-AMS-022772
A4-207	2.1	4.7	Plant fragment	4170	35	4830–4580	4710	D-AMS-022773
A6-156	1.6	4.9	Plant fragment	1580	30	1540–1400	1470	D-AMS-022774
A6-240	2.4	4.1	Plant fragment	1870	35	1880–1720	1810	D-AMS-022775
A6-250	2.5	4.0	Plant fragment	2255	40	2350–2150	2240	D-AMS-019972
A6-280	2.8	3.7	Plant fragment	3280	35	3590–3410	3510	D-AMS-022776
B2-270	2.7	3.9	Plant fragment	5315	35	6200–5990	6090	D-AMS-019975
B3-90	0.9	5.9	Plant fragment	1035	30	1050–910	950	D-AMS-022785
B3-223	2.2	4.6	Plant fragment	3695	55	4230–3880	4040	D-AMS-022786
B3-317	3.2	3.6	Plant fragment	5665	45	6560–6320	6450	D-AMS-019974
B4-130	1.3	5.2	Plant fragment	1630	45	1690–1410	1530	D-AMS-022784
B5-140	1.4	5.5	Plant fragment	1790	45	1830–1570	1720	D-AMS-022780
B5-178	1.8	5.1	Plant fragment	2770	65	3030–2760	2880	D-AMS-022781
B5-225	2.3	4.6	Plant fragment	4535	35	5310–5050	5260	D-AMS-022782
B5-230	2.3	4.6	Plant fragment	4805	60	5650–5330	5520	D-AMS-019973
B5-270	2.7	4.2	Plant fragment	4930	35	5730–5600	5650	D-AMS-022783
B6-180	1.8	5.4	Plant fragment	1770	45	1820–1570	1680	D-AMS-022777
B6-205	2.1	5.1	Plant fragment	1915	50	1990–1730	1860	D-AMS-022778
B6-255	2.6	4.6	Plant fragment	3945	70	4570–4160	4390	D-AMS-022779
C3-285	2.9	4.4	Wood fragment	5665	50	6600–6310	6450	D-AMS-019976
D2-220	2.2	5.7	Plant fragment	3710	35	4150–3930	4050	D-AMS-019979
D2-340	3.4	4.5	Plant fragment	3395	45	3830–3500	3640	D-AMS-019978
D4-180	1.8	6.6	Plant fragment	2090	55	2300–1900	2060	D-AMS-022787
D4-238	2.4	6.0	Plant fragment	3890	40	4420–4160	4330	D-AMS-022788
D4-335	3.4	5.0	Plant fragment	5500	40	6400–6210	6300	D-AMS-019977

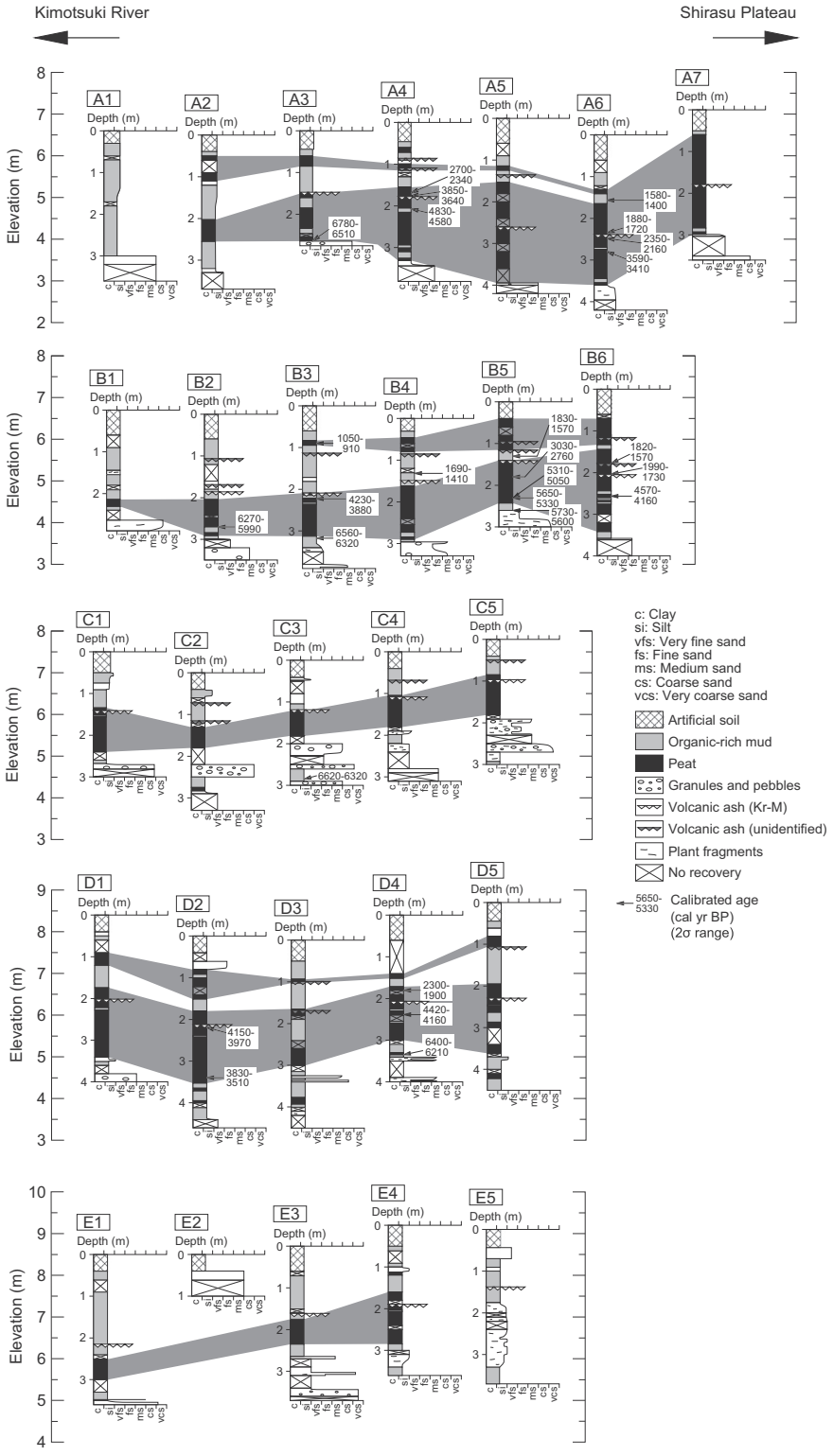

Fig. 5. Columnar sections arranged by transect; boreholes are numbered in ascending order with distance from the river. The shading indicates the lateral correlation of peat.

rich mud deposition appears to have started around or after 2000 cal yr BP (Fig. 5).

4.4. Age–depth model

Age–depth models were constructed for 9 sites based on radiocarbon ages and the estimated Kr-M age of 4000 cal yr BP (Fig. 6). Omitted from the age–depth models were artificial soils (dashed lines in Fig. 6), because these may have been imported for agricultural purposes. Also excluded from the age–depth models were the previously mentioned radiocarbon ages showing age-reversals at sites A6 and B5.

The age–depth models at boreholes A4, A6, B4, B5, B6, and D4 have a similar shape that is typical of the study area (Fig. 6). Sedimentation rates decreased considerably around 4000 cal yr BP and were almost

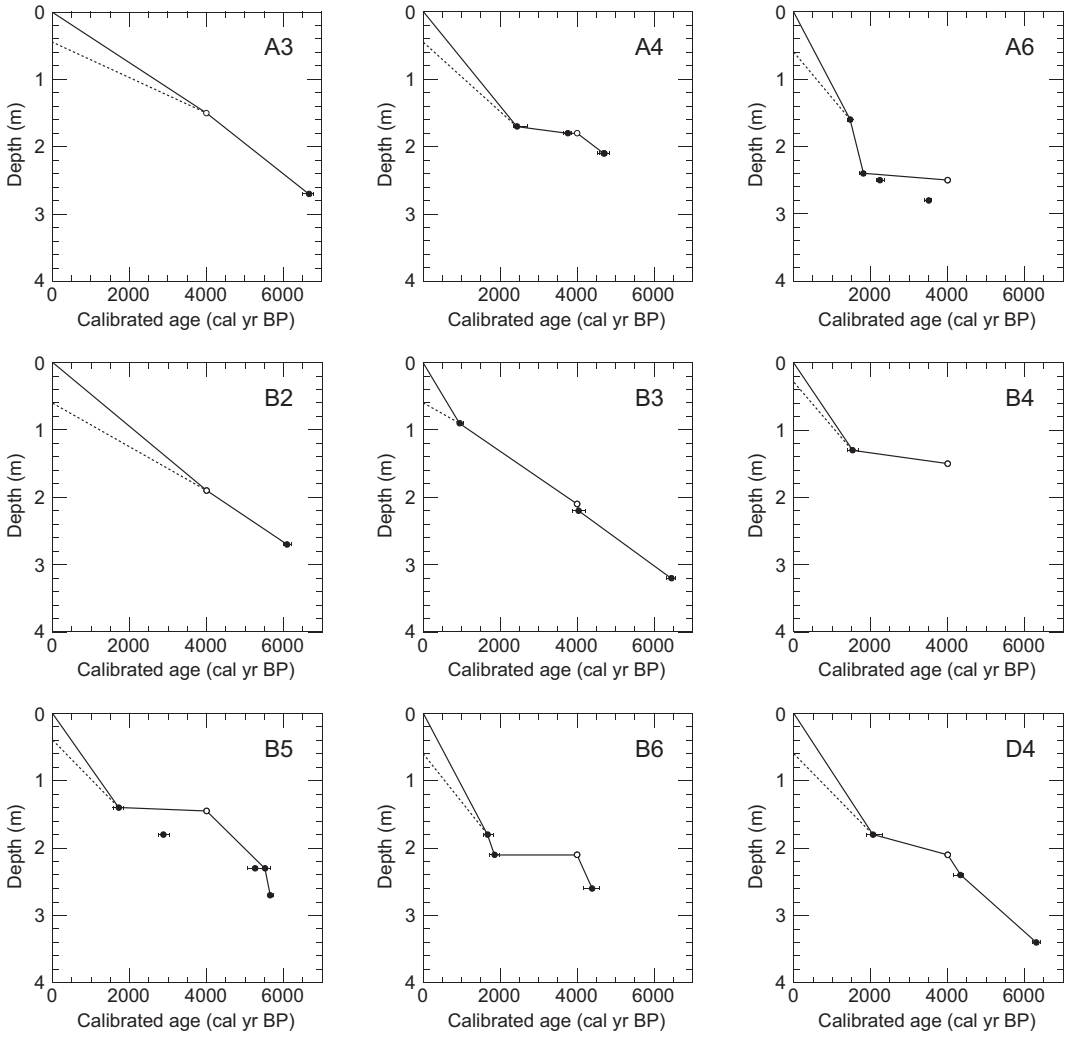

Fig. 6. Age–depth models of selected auger cores, dashed lines are used where age-depth models omitted artificial soil. The black and white dots represent radiocarbon ages and Kr-M, respectively. The estimated depositional age of Kr-M is 4000 cal yr BP based on an average of radiocarbon dates at sites A4, B3, and D2.

negligible until 2000–1500 cal yr BP. This decreasing sedimentation rate was not clear at boreholes A3, B2, and B3 because radiocarbon ages from these cores were not obtained within several decimeters above the Kr-M. Sedimentation rates increased after 2000–1500 cal yr BP as clearly shown in the age–depth models, even those omitting artificial soil (Fig. 7A). The sedimentation rate increase coincides with the onset of organic-rich mud deposition at boreholes A4 and B4, and the resumption of peat deposition at boreholes A6 and B6 (Figs. 5 and 6).

5. Discussion

5.1. Evolution of the delta plain and influence of allogenic controls

5.1.1. 7000–6000 cal yr BP

The basal delta plain consists of large-scale crevasse splay deposits overlain by peat (Fig. 5). The crevasse splay was abandoned at 7000–6000 cal yr BP based on the predominant age of sediments above the basal sands. Although a small-scale crevasse splay in transect C formed after 6500 cal yr BP, its formation and abandonment appear brief because the peat thickness between the sand layer and the Kr-M is similar to that in other transects. The relatively younger ages (5500 cal yr BP) near and above the basal sands at borehole B5 may be due to downward penetration of roots. The abandonment of crevasse splays at 7000–6000 cal yr BP decreased clastic input into the flood-basin and peat formation began (e.g. Morozova and Smith, 2000).

The fluvial aggradation may in part be due to early to middle Holocene rapid sea-level rise commonly observed in other low-gradient coastal floodplains (e.g. Aslan and Autin, 1999) and abandonment of the crevasse splays at 7000–6000 cal yr BP coincides with the deceleration of eustatic sea-level rise around 7000 cal yr BP (Fleming et al., 1998; Peltier, 2002, 2004; Lambeck et al., 2014). The rate of relative sea-level rise in embayments in Japan also decreased at 7000–6000 cal yr BP because the relative sea-level change in the far-field strongly reflects the eustatic sea-level change (Fleming et al., 1998). Consequently, both the formation and abandonment of crevasse splays in the study area appear strongly controlled by eustatic sea-level changes.

Crevasse splays may also be associated with post-eruption erosion from deforestation. The deposition of the Koya pyroclastic flows and K-Ah ash fall around 7300 cal yr BP, and the Ik-P around 6400 cal yr BP coincide with the formation and abandonment of crevasse splays. The thickness of these deposits in the upstream catchment ranges from a few decimeters and up to 1 m for the Ik-P (Machida and Arai, 1978; Kawabe and Sakaguchi, 2005; Fujiwara and Suzuki-Kamata, 2013). Matsushita (2002) found the Kikai-Akahoya eruption destroyed vegetation around the study area that required a few centuries to recover. Post-eruption erosion from deforestation may have increased sediment supply to the river and caused bed aggradation that resulted in crevassing (Makaske et al., 2009).

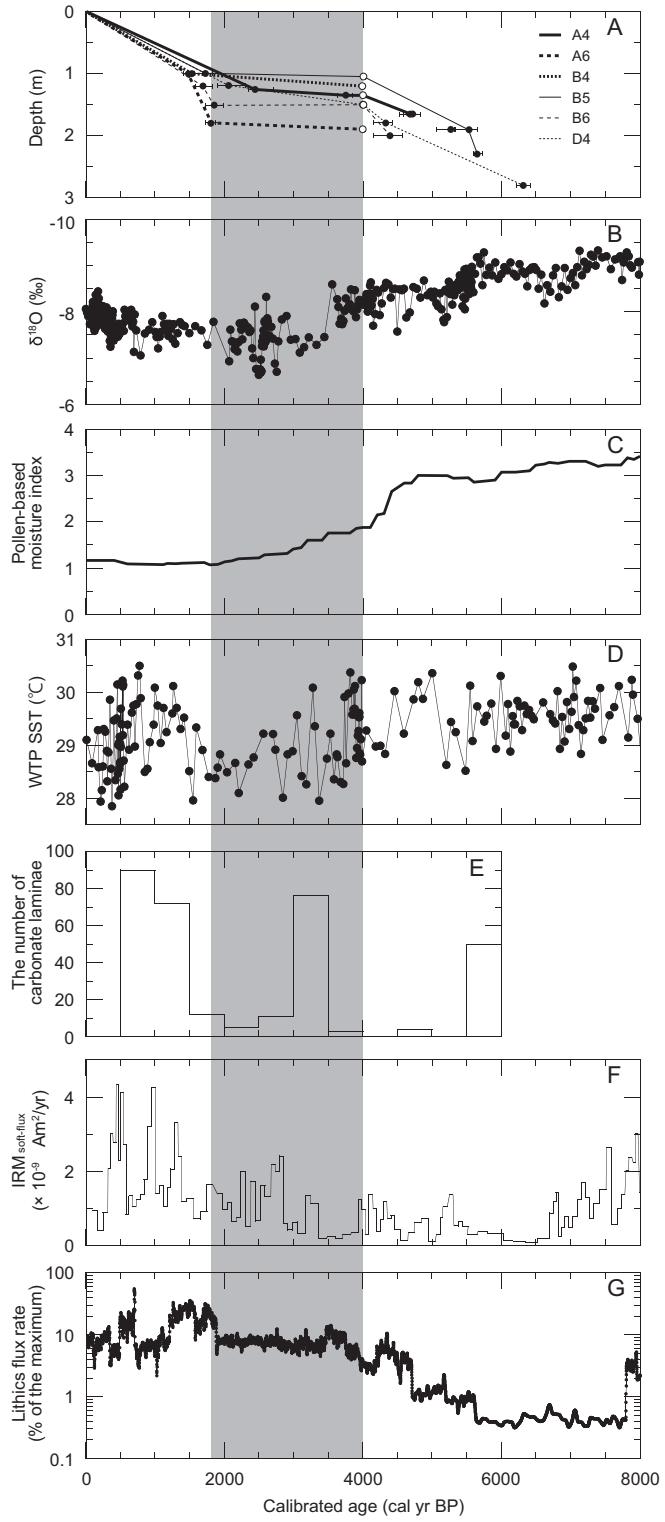

Fig. 7. A comparison of representative age–depth models for the Kimotsuki delta plain with paleoclimate proxies. A. Age–depth models representative of the study area. The depth models exclude the artificial soil. B. A proxy for EASM precipitation based on δ18O values of stalagmite D4, Dongge Cave, China (Dykoski et al., 2005). Higher δ18O values are associated with a weaker summer monsoon, including a remarkable positive shift around 4000 cal yr BP. C. Pollen-based moisture index in China (Zhao et al., 2009). Higher values indicate more humid conditions. D. Sea surface temperatures in the western tropical Pacific reconstructed from Mg/Ca of *Globigerinoides ruber* (core MD81; Stott et al., 2004). E. The number of carbonate laminae in a Galápagos lake sediment record, counted in 500 year bins (Thompson et al., 2017). The number of carbonate laminae reflects the frequency of La Niña events. F. Geophysical parameter $IRM_{soft\text{-}flux}$ that represents the flux of soil-derived magnetic minerals preserved in stalagmite HS4 (Zhu et al., 2017). Abrupt enhancements in $IRM_{soft\text{-}flux}$ are related to an increased frequency of extreme precipitation events. G. Lithics flux rate in marine sediments relative to maximum flux, obtained from a core off the coast of Peru (Rein et al., 2005). The increased lithics flux reflects more frequent and intense El Niño events. The shaded area denotes a period of negligible sedimentation on the Kimotsuki delta plain.

5.1.2. 6000–4000 cal yr BP

The age-depth models indicate continuous peat formation during 6000–4000 cal yr BP (Fig. 7A). The $\delta^{18}O$ values from stalagmite records (Fig. 7B; Dykoski et al., 2005; Hu et al., 2008) and lake-level proxies in China (Xiao et al., 2008; Wu et al., 2012; Goldsmith et al., 2017) shows a decrease in precipitation from a weakened EASM at around 5000 cal yr BP. A weaker Walker Circulation due to the weakened EASM at that time (Liu et al., 2000; Tian et al., 2017) may have led to a decreased frequency of La Niña events (Fig. 7E; Thompson et al., 2017) and increased El Niño activity (Fig. 7G; Moy et al., 2002; Rein et al., 2005). However, these climate changes do not seem to have an influence on peat formation in the study area.

5.1.3. 4000–2000 cal yr BP

The age–depth models show that peat deposition ceased around 4000 cal yr BP and negligible sedimentation occurred until 2000–1500 cal yr BP (Figs. 5 and 6). The cessation of peat coincides with a large decrease in peat LOI values around the Kr-M (Fig. 4). Peat formation is generally controlled by clastic sediment input into a floodbasin and water levels (Bohacs and Suter, 1997). Comparison of the age–depth models and sedimentary columns indicates that clastic sedimentation and peat deposition were negligible from 4000 to 2000 cal yr BP (Figs. 5 and 6), suggesting that the peatlands dried out.

While the deposition of the Kr-M is of similar age, such a thin tephra layer (a few to several centimeters thick) is unlikely to impact peatland vegetation substantially, but may have local effects (e.g. Hotes et al., 2001). One possible cause of peatland drying is relative sea-level fall during the middle to late Holocene from isostatic rebound (Yokoyama et al., 2012, 2016), and may have lowered the floodbasin water level. Relative sea level near the river mouth around 6000 cal yr BP was possibly 2 m higher than present and fell afterwards (Okuno et al., 2014).

However, peat cessation appears to be associated with decreased precipitation. Although climate conditions in central and southern Japan are generally not suitable for widespread peatlands on coastal floodplains and delta plains, abundant spring water from the Shirasu Plateau facilitated development of peatlands in the Kimotsuki lowland (Sakaguchi, 1960; Arizono, 1985). The peatlands and springs in the study area cannot be maintained without abundant precipitation, and decreased precipitation may have caused the drying of peatlands ca. 4000 cal yr BP.

Decreased precipitation from a weakened EASM at 5600–3000 cal yr BP has been inferred from $\delta^{18}O$ values from abundant stalagmite records in China (Fig. 7B; Dykoski et al., 2005; Hu et al., 2008) and pollen-based moisture index in China (Fig. 7C; Zhao et al., 2009), with the most prominent decrease around 4000 cal yr BP. Decreased precipitation is also indicated by lake-level proxies in China where lake levels fell at around 4000 cal yr BP (Xiao et al., 2008; Zhao et al., 2010; Wu et al., 2012). Decreased temperatures in the middle to late Holocene reported in many areas of Japan including Kyushu (Sakaguchi, 1961; Yasuda, 1974; Hatanaka, 1985; Kitagawa and Yasuda, 2008; Kitagawa et al., 2009) may partially reflect a weakening EASM. The decreased precipitation from a weakened EASM around 4000 cal yr BP may have reduced the spring water discharge from the

Shirasu Plateau and dried out the peatlands.

The strengthened El Niño activity after 4000 cal yr BP (Fig. 7G; Rein et al., 2005) coincides with the weakened EASM at that time (Fig. 7B; Dykoski et al., 2005; Conroy et al., 2008). Some studies indicate that the frequency of La Niña events also increased at around 3000 cal yr BP (Fig. 7E; Makou et al., 2010; Thompson et al., 2017). Although the phase relationship between ENSO activity and the magnitude and frequency of tropical storms and typhoons is not straightforward (Camargo et al., 2007), the frequent storms in China at around 3000 cal yr BP (Fig. 7F; Zhu et al., 2017) may be related to the frequent La Niña events. However, the sea surface temperatures (SSTs) in the western tropical Pacific was relatively low at 4000–2000 cal yr BP (Fig. 7D) and less oceanic heat and moisture from the western tropical Pacific and Kuroshio extension may have been supplied to the tropical storms and typhoons. Accordingly, the magnitude of storm events may have been relatively small.

5.1.4. After 2000 cal yr BP

Resumption of peat deposition or initiation of organic-rich mud deposition occurred at 2000–1500 cal yr BP (Figs. 5 and 6). The thickening of organic-rich mud toward the Kimotsuki River along transects A, B, C, and E indicates that the organic-rich mud deposition is associated with overbank sedimentation (Fig. 5). The unclear relationship between organic-rich mud thickness and distance from the river along transect D may reflect the effects of local topography on overbank sedimentation (e.g. Nicholas and Walling, 1997).

Peat deposition at boreholes furthest from the Kimotsuki River, such as borehole B6, suggest that floodbasin water levels rose due to increased precipitation. However, the increased precipitation around 2000 cal yr BP is not apparent in stalagmite $\delta^{18}O$ records (Fig. 7B; Dykoski et al., 2005; Hu et al., 2008) and pollen-based moisture index in China (Fig. 7C; Zhao et al., 2009). The high SSTs in the western tropical Pacific around 2000 cal yr BP (Fig. 7D; Jiang et al., 2000; Stott et al., 2004) may have increased SSTs of the Kuroshio extension, possibly increasing the transfer of oceanic heat and moisture to coastal areas of the EASM region (Park, 2017).

The organic-rich mud deposition appears to correspond to the increased magnitude and frequency of floods indicated by high $IRM_{soft\text{-}flux}$ values of stalagmite HS4 in China (Fig. 7F; Zhu et al., 2017). The frequent La Niña events (Fig. 7; Makou et al., 2010; Thompson et al., 2017) and the increased SSTs of the Kuroshio extension due to the high SSTs in the western tropical Pacific (Fig. 7D; Jiang et al., 2000; Stott et al., 2004) may have increased the magnitude and frequency of tropical storms and typhoons. The similar ages of peat resumption and initiation of organic-rich mud deposition also suggest that these changes in sedimentary environment have the same cause. The enhanced storminess is not recorded in the stalagmite $\delta^{18}O$ records (Fig. 7B; Dykoski et al., 2005; Hu et al., 2008) or pollen-based moisture index in China (Fig. 7C; Zhao et al., 2009) because they mainly reflect the amount of summer monsoon precipitation.

The organic-rich mud deposition may be also influenced by increased sediment discharge from man-made deforestation. Pollen assemblages indicate that secondary forest characterized by *Pinus* rapidly expanded at 2000–1000 cal yr BP in Japan (Tsukada, 1981; Hatanaka, 1985), and the human activities in the upstream catchment may have increased sediment discharge. However, it is difficult to evaluate the influence of human activities because the history of human activities in the upstream catchment of the Kimotsuki River has not been well investigated.

5.2. Comparisons to and implications for the evolution of other floodplains

5.2.1. Weakened EASM in the middle to late Holocene

In the Ishikari and Shiribeshi-Toshibetsu River lowlands of northern Japan, decreased precipitation from a weakened EASM may have led to near-cessation of overbank deposition, followed by peat initiation, particularly at 5600–5000 and 4100–3600 cal yr BP (Ishii et al., 2016; Ishii, 2017a). In contrast, the fluvial aggradation in the Kimotsuki lowland nearly stopped much earlier at 7000–6000 cal yr BP, followed by peat formation. The weakening of fluvial activity from decreased precipitation at 5600–3600 cal yr BP in northern Japan could not be detected in the Kimotsuki lowland. This suggests that a weakened EASM in the middle to late Holocene may not have substantially influenced the development of coastal floodplains and delta plains where fluvial aggradation decreased in accordance with a reduction and ending of rapid sea-level rise around 7000 cal yr BP.

Water and sediment supplies from the upstream catchment and relative sea level at the river mouth generally determine the rate of fluvial aggradation (Makaske et al., 2009; Blum et al., 2013; Nijhuis et al., 2015). The fluvial aggradation ceased in the Kimotsuki lowland probably due to deceleration of sea-level rise and decreased sediment supply at 7000–6000 cal yr BP. In contrast, fluvial aggradation continued in the Ishikari lowland although the relative sea level did not rise after 6000 cal yr BP (Okuno et al., 2014; Ishii et al., 2016; Ishii, 2017b). Abundant sediment supply from the upstream catchment may have promoted fluvial aggradation after 7000 cal yr BP in the Ishikari lowland. However, it is difficult to identify the factors responsible for the differences between the two cases because sediment supply is influenced by many factors such as geology, catchment slope, and sediment transport pathways.

The weakening EASM around 4000 cal yr BP had a critical influence on the drying of peatlands in the Kimotsuki lowland. In contrast to those in the northern part of Honshu and Hokkaido, the peatlands may have been susceptible to the decreased precipitation because climate conditions in central and southern Japan are generally not suitable for widespread peatlands on coastal floodplains and delta plains. This type of response to the decreased precipitation may be specific to the Kimotsuki lowland.

5.2.2. Strong La Niña and man-made deforestation in the late Holocene

An increase in overbank sedimentation after around 2000 cal yr BP like that in the Kimotsuki lowland has also been observed also in many other Japanese lowlands, including the Kawachi Plain (Yasuda, 1978), Yahagi River lowland (Kawase, 1998), Nobi Plain (Ono, 2004), Nara basin (Itoh et al., 2017). These studies inferred that the active fluvial deposition was highly influenced by climate change (Yasuda, 1978; Kawase, 1998; Ono, 2004), increased sediment discharge from man-made deforestation (Kawase, 1998; Hasada, 2015; Itoh et al., 2017), or both. Although the increase in precipitation or storminess after 2000 cal yr BP in Japan has not been reported, the results of this study suggest that the increased precipitation and enhanced fluvial activity are related to the increased frequency of La Niña events (Fig. 7E; Makou et al., 2010; Thompson et al., 2017) and the high SSTs in the western tropical Pacific (Fig. 7D; Jiang et al., 2000; Stott et al., 2004).

In the Nobi Plain, the sediment storage on the delta plain during the last 6000 years is estimated for every 1000-year interval (Hasada, 2015). Hasada (2015) suggested that the increase in sediment storage after 1000 cal yr BP is related to man-made deforestation from fuelwood consumption for ceramic production after 1200 cal yr BP (Hasada, 2015). In contrast, a significant increase in sediment storage is not reported at 2000–1000 cal yr BP. More accurate estimation of sediment storage on the delta plain or detailed history of the delta plain evolution may be needed to detect the active fluvial deposition after 2000–1500 cal yr BP.

Increased fluvial activity was also detected from loss on ignition of peat around 1400–1300 cal yr BP and possibly thereafter in the Ishikari lowland, where human activities were negligible before the 19th century (Ishii et al., 2017). However, peat formation continued without significant fluvial deposition, although the Ishikari River floodplain seems to be more aggradational probably because of its large sediment supply. The absence of thick fluvial deposits after ca. 2000 cal yr BP may be related to its smaller number of typhoon landfalls on Hokkaido

and/or almost absence of human activities.

The stalagmite HS4 record in China (Zhu et al., 2017) indicates that large storm events frequently occurred after ca. 2000 cal yr BP in China (Fig. 7F). Slackwater deposits in the upstream reaches of Yellow and Yangtze rivers also demonstrate the occurrence of large floods after 2000 cal yr BP (Huang et al., 2007, 2013; Guo et al., 2016). Increased fluvial activity after 2000 cal yr BP may be common in coastal floodplains and delta plains in the East Asia region.

6. Conclusions

This study details delta plain evolution in the Kimotsuki lowland, and helped determine the influence of regional climate change on a southern Japanese (Kyushu) fluvial system. Fluvial aggradation in the study area nearly stopped at 7000–6000 cal yr BP, when the rate of eustatic sea-level rise slowed considerably. Peatlands were established thereafter, but decreased precipitation from a weakened EASM caused drying of peatlands around 4000 cal yr BP. The near-cessation of peat between 4000 and 2000 cal yr BP is consistent persistent low monsoon precipitation. The increased precipitation due to the frequent La Niña events and the high SSTs in the western tropical Pacific may have caused the resumption of peat deposition at areas further from the Kimotsuki River at 2000–1500 cal yr BP. Meanwhile, active overbank sedimentation after ca. 2000–1500 cal yr BP in Japanese floodplains and delta plains including the Kimotsuki lowland may be associated with the enhanced storminess due to the increased frequency of La Niña events and the high SSTs in the western tropical Pacific. The results suggest that regional climate change in the late Holocene has a potential to control the evolution of coastal floodplains and delta plains.

Acknowledgments

I am grateful to Hiroyuki Kitagawa of Nagoya University for preparing graphite samples for ^{14}C analysis. I am also grateful to the landowners in the Kimotsuki lowland for allowing us access to their land. I thank the officials of the Kimotsuki town for providing columnar sections. I greatly appreciate the assistance of Kazuki Kumazawa in the field. Kazuaki Hori of Nagoya University is acknowledged for useful comments on an earlier version of the manuscript. The manuscript was greatly improved by comments from two anonymous reviewers. This work was supported by a Grant-in-Aid for JSPS Fellows (15J01971).

References

Arizono, S., 1985. Farming systems of southern Kyushu in the mid-19th century. Geogr. Rev. Jpn 58A, 789–806 (in Japanese with English abstract).
Aslan, A., Autin, W.J., 1999. Evolution of the Holocene Mississippi River floodplain, Ferriday, Louisiana: insights on the origin of fine-grained floodplains. J. Sediment. Res. 69, 800–815.
Aslan, A., Blum, M.D., 1999. Contrasting styles of Holocene avulsion, Texas Gulf Coastal Plain, USA. In: Smith, N.D., Rogers, J.J. (Eds.), Fluvial Sedimentology VI: Special Publication of Internal Association of Sedimentologists. 28. pp. 193–209.
Blum, M.D., Törnqvist, T.E., 2000. Fluvial responses to climate and sea-level change: a review and look forward. Sedimentology 47, 2–48.
Blum, M., Martin, J., Milliken, K., Garvin, M., 2013. Paleovalley systems: Insights from Quaternary analogs and experiments. Earth Sci. Rev. 116, 128–169.
Bohacs, K., Suter, J., 1997. Sequence stratigraphic distribution of coaly rocks: Fundamental controls and paralic examples. AAPG Bull. 81, 1612–1639.
Bronk Ramsey, C., 2009. Bayesian analysis of radiocarbon dates. Radiocarbon 51, 337–360.
Camargo, S.J., Robertson, A.W., Gaffney, S.J., Smyth, P., Ghil, M., 2007. Cluster analysis of typhoon tracks. Part II: large-scale circulation and ENSO. J. Clim. 20, 3654–3676.
Conroy, J.L., Overpeck, J.T., Cole, J.E., Shanahan, T.M., Steinitzu-Kannan, M., 2008. Holocene changes in eastern tropical Pacific climate inferred from a Galápagos lake sediment record. Quat. Sci. Rev. 27, 1166–1180.
Dykoski, C.A., Edwards, R.L., Cheng, H., Yuan, D., Cai, Y., Zhang, M., Lin, Y., Qing, J., An, Z., Revenaugh, J., 2005. A high-resolution, absolute-dated Holocene and deglacial Asian monsoon record from Dongge Cave, China. Earth Planet. Sci. Lett. 233, 71–86.
Fleming, K., Johnston, P., Zwartz, D., Yokoyama, Y., Lambeck, K., Chappell, J., 1998. Refining the eustatic sea-level curve since the Last Glacial Maximum using far- and intermediate-field sites. Earth Planet. Sci. Lett. 163, 327–342.
Fujiwara, M., Suzuki-Kamata, K., 2013. Glass composition and emplacement mode of Koya pyroclastic-flow deposit and its proximal equivalent. Bull. Volc. Soc. Japan 58, 489–498 (in Japanese with English abstract).
Goldsmith, Y., Broecker, W.S., Xu, H., Polissar, P.J., deMenocal, P.B., Porat, N., Lan, J., Cheng, P., Zhou, W., An, Z., 2017. Northward extent of East Asian monsoon covaries with intensity on orbital and millennial timescales. Proc. Natl. Acad. Sci. U. S. A. 114, 1817–1821.
Grimm, E.C., Maher Jr., L.J., Nelson, D.M., 2009. The magnitude of error in conventional bulk-sediment radiocarbon dates from central North America. Quat. Res. 72, 301–308.
Guo, Y., Huang, C.C., Zhou, Y., Pang, J., Zha, X., Zhou, L., Mao, P., 2016. Extraordinary flood events and the response to monsoonal climatic change during the last 3000 years along the middle Yangtze River valley, China. Palaeogeogr. Palaeoclimatol. Palaeoecol. 462, 70–84.
Hasada, K., 2015. Reconstruction of three-dimensional stratigraphic architecture and sediment storage on the Nobi Plain based on borehole data analysis using GIS. Geogr. Rev. Jpn Series A 88, 118–137 (in Japanese with English abstract).
Hatanaka, K., 1985. Palynological studies on the vegetational succession since the Würm glacial age in Kyushu and adjacent areas. J. Fac. Lit., Kitakyushu Univ. (Series B) 18, 29–71.
Hori, K., Usami, S., Ueda, H., 2011. Sediment facies and Holocene deposition rate of near-coastal fluvial systems: An example from the Nobi Plain, Japan. J. Asian Earth Sci. 41, 195–203.
Hotes, S., Poschlod, P., Sakai, H., Inoue, T., 2001. Vegetation, hydrology, and development of a coastal mire in Hokkaido, Japan, affected by flooding and tephra deposition. Can. J. Bot. 79, 341–361.
Hu, C., Henderson, G.M., Huang, J., Xie, S., Sun, Y., Johnson, K.R., 2008. Quantification of Holocene Asian monsoon rainfall from spatially separated cave records. Earth Planet. Sci. Lett. 266, 221–232.
Huang, C.C., Pang, J., Zha, X., Su, H., Jia, Y., Zhu, Y., 2007. Impact of monsoonal climatic change on Holocene overbank flooding along Sushui River, middle reach of the Yellow River, China. Quat. Sci. Rev. 26, 2247–2264.
Huang, C.C., Pang, J., Zha, X., Zhou, Y., Yin, S., Su, H., Zhou, L., Yang, J., 2013. Extraordinary hydro-climatic events during the period AD 200 – 300 recorded by slackwater deposits in the upper Hanjiang River valley, China. Palaeogeogr. Palaeoclimatol. Palaeoecol. 374, 274–283.
Iseki, H., 1962. Basic issues for researches of alluvial plains. Journal of Faculty of Literature, Nagoya University. History 24, 51–74 (in Japanese).
Ishii, Y., 2017a. Holocene floodplain evolution in the Shirbeshi-Toshibetsu River lowland, northern Japan. Geomorphology 292, 25–34.
Ishii, Y., 2017b. Bay-head delta progradation and delta plain development in the Ishikari lowland. Geogr. Revi. Japan Series A 90, 105–124 (in Japanese with English abstract).
Ishii, Y., Hori, K., Momohara, A., Nakanishi, T., Hong, W., 2016. Middle to late-Holocene decreased fluvial aggradation and widespread peat initiation in the Ishikari lowland (northern Japan). The Holocene 26, 1924–1938s.
Ishii, Y., Hori, K., Momohara, A., 2017. Middle to late Holocene flood activity estimated from loss on ignition of peat in the Ishikari lowland, northern Japan. Glob. Planet. Chang. 153, 1–15.
Itoh, N., Hori, K., Takada, M., 2017. Latest pleistocene to holocene alluvial basin construction: An example from the Nara Basin, central Japan. Quat. Int. 455, 102–112.
Jiang, Z., Wang, P., Saito, Y., Wang, J., Pflaumann, U., Oba, T., Cheng, X., 2000. Holocene variability of the Kuroshio Current in the Okinawa sTrough, northwestern Pacific Ocean. Earth Planet. Sci. Lett. 184, 305–309.
Kawabe, Y., Sakaguchi, K., 2005. Geology of the Kaimon Dake district. Quadrangle Series, 1:50,000. Geological Survey of Japan, AIST, Tsukuba, pp. 82 (in Japanese with English abstract).
Kawase, K., 1998. Late Holocene paleoenvironmental changes in the Yahagi River lowlands, central Japan. Geogr. Rev. Jpn 71A, 411–435 (in Japanese with English abstract).
Kitagawa, J., Yasuda, Y., 2008. Development and distribution of Castanea and Aesculus culture during the Jomon Period in Japan. Quat. Int. 184, 41–55.
Kitagawa, Y., Yoshikawa, S., Takahara, H., 2009. Vegetation history in Osaka Bay watershed areas during the Holocene reconstructed from pollen analysis of Yumeshima-oki core, Osaka Bay, Japan. Quaternary Res. (*Daiyonki Kenkyuu*) 48, 351–363 (in Japanese with English abstract).
Kyushu Regional Development Bureau, 2012. Kimotsukigawa Suikei Kasen Seibi Keikaku (River Improvement Plan of the Kimotsuki River). (in Japanese).
Lambeck, K., Rouby, H., Purcell, A., Sun, Y., Sambridge, M., 2014. Sea level and global ice volumes from the Last Glacial Maximum to the Holocene. Proc. Natl. Acad. Sci. U. S. A. 111, 15296–15303.
Liu, Z., Kutzbach, J., Wu, L., 2000. Modeling climate shift of El Niño variability in the Holocene. Geophys. Res. Lett. 27, 2265–2268.
Machida, H., Arai, F., 1978. Akahoya ash: a Holocene widespread tephra erupted from the Kikai caldera, southern Kyushu, Japan. Quat. Res. (*Daiyonki Kenkyuu*) 17, 143–163 (in Japanese with English abstract).
Makaske, B., Smith, D.G., Berendsen, H.J.A., de Boer, A.G., van Nielen-Kiezebrink, M.F., Locking, T., 2009. Hydraulic and sedimentary processes causing anastomosing morphology of the upper Columbia River, British Columbia, Canada. Geomorphology 111, 194–205.
Makou, M.C., Eglinton, T.I., Oppo, D.W., Hughen, K.A., 2010. Postglacial changes in El Niño and La Niña behavior. Geology 38, 43–46.
Marcott, S.A., Shakun, J.D., Clark, P.U., Mix, A.C., 2013. A reconstruction of regional and global temperature for the past 11,300 years. Science 339, 1198–1201.
Marriner, N., Flaux, C., Kaniewski, D., Morhange, C., Leduc, G., Moron, V., Chen, Z., Gasse, F., Empereur, J.-Y., Stanley, J.-D., 2012a. ITCZ and ENSO-like pacing of Nile delta hydro-geomorphology during the Holocene. Quat. Sci. Rev. 45, 73–84.

Marriner, N., Flaux, C., Morhange, C., Kaniewski, D., 2012b. Nile Delta's sinking past: Quantifiable links with Holocene compaction and climate-driven changes in sediment supply? Geology 40, 1083–1086.
Matsushita, M., 2002. Vegetation changes under the influence of the Kikai-Akahoya eruption in Osumi Peninsula, southerna Kyushu, Japan. Quat. Res. (*Daiyonki Kenkyuu*) 41, 301–310 (in Japanese with English abstract).
Moriwaki, H., Nakamura, N., Nagasako, T., Lowe, D.J., Sangawa, T., 2016. The role of tephras in developing a high-precision chronostratigraphy for palaeoenvironmental reconstruction and archaeology in southern Kyushu, Japan, since 30,000 cal. BP: An integration. Quat. Int. 397, 79–92.
Morozova, G.S., Smith, N.D., 2000. Holocene avulsion styles and sedimentation patterns of the Saskatchewan River, Cumberland Marshes, Canada. Sediment. Geol. 130, 81–105.
Moy, C.M., Seltzer, G.O., Rodbell, D.T., Anderson, D.M., 2002. Variability of El Niño/Southern Oscillation activity at millennial timescales during the Holocene epoch. Nature 420, 162–165.
Nagasako, T., Okuno, M., Moriwaki, H., Arai, F., Nakamura, T., 1999. Paleogeography and tephras of the Kimotsuki Lowland, southern Kyushu, Japan, in the middle to late Holocene. Quat. Res. (*Daiyonki Kenkyuu*) 38, 163–173 (in Japanese with English abstract).
Nakada, M., Yonekura, N., Lambeck, K., 1991. Late Pleistocene and Holocene sea-level changes in Japan: implications for tectonic histories and mantle rheology. Palaeogeogr. Palaeoclimatol. Palaeoecol. 85, 107–122.
Nicholas, A.P., Walling, D.E., 1997. Modelling flood hydraulics and overbank deposition on river floodplains. Earth Surf. Process. Landf. 22, 59–77.
Nijhuis, A.G., Edmonds, D.A., Caldwell, R.L., Cederberg, J.A., Slingerland, R.L., Best, J.L., Parsons, D.R., Robinson, R.A.J., 2015. Fluvio-deltaic avulsions during relative sea-level fall. Geology 43, 719–722.
Okuno, M., 2001. Tephrochronology and radiocarbon chronology in Japan. Quat. Res. (*Daiyonki Kenkyuu*) 40, 461–470 (in Japanese with English abstract).
Okuno, J., Nakada, M., Ishii, M., Miura, H., 2014. Vertical tectonic crustal movements along the Japanese coastlines inferred from late Quaternary and recent relative sea-level changes. Quat. Sci. Rev. 91, 42–61.
Ono, E., 2004. Factors affecting late Holocene marine regression in the Nobi Plain, central Japan. Geogr. Rev. Jpn 77, 77–98 (in Japanese with English abstract).
Park, J., 2017. Solar and tropical ocean forcing of late-Holocene climate change in coastal East Asia. Palaeogeogr. Palaeoclimatol. Palaeoecol. 469, 74–83.
Peltier, W.R., 2002. On eustatic sea level history: Last Glacial Maximum to Holocene. Quat. Sci. Rev. 21, 377–396.
Peltier, W.R., 2004. Global glacial isostasy and the surface of the ice-age Earth: The ICE-5G (VM) model and GRACE. Annu. Rev. Earth Planet. Sci. 32, 111–149.
Pennington, B.T., Bunbury, J., Hovius, N., 2016. Emergence of civilization, changes in fluvio-deltaic style, and nutrients redistribution forced by Holocene sea-level rise. Geoarchaeology 31, 194–210.
Pennington, B.T., Sturt, F., Wilson, P., Rowland, J., Brown, A.G., 2017. The fluvial evolution of the Holocene Nile Delta. Quat. Sci. Rev. 170, 212–231.
Reimer, P.J., Bard, E., Bayliss, A., Beck, J.W., Blackwell, P.G., Bronk Ramsey, C., Buck, C.E., Cheng, H., Edwards, R.L., Friedrich, M., Grootes, P.M., Guilderson, T.P., Haflidason, H., Hajdas, I., Hatté, C., Heaton, T.J., Hoffmann, D.L., Hogg, A.G., Hughen, K.A., Kaiser, K.F., Kromer, B., Manning, S.W., Niu, M., Reimer, R.W., Richards, D.A., Scott, E.M., Southon, J.R., Staff, R.A, Turney, C.S.M., van der Plicht, J., 2013. IntCal13 and Marine13 radiocarbon age calibration curves 0–50,000 years cal BP. Radiocarbon 55, 1869–1887.
Rein, B., Lückge, A., Reinhardt, L., Sirocko, F., Wolf, A., Dullo, W.C., 2005. El Niño variability off Peru during the last 20,000 years. Paleoceanography 20, PA4003.
Saito, Y., Yang, Z., Hori, K., 2001. The Huanghe (Yellow River) and Changjiang (Yangtze River) deltas: a review on their characteristics, evolution and sediment discharge during the Holocene. Geomorphology 41, 219–231.
Sakaguchi, Y., 1960. On the peat layers of the Kimotsuki alluvial plain. In: Miscellaneous Reports of the Research Institute for Natural Resources. 52–53. pp. 93–95 (in Japanese with English abstract).
Sakaguchi, Y., 1961. Climatic changes of northern Japan during the Holocene epoch. Geogr. Rev. Jpn 34, 259–268 (in Japanese with English abstract).
Sakaguchi, Y., 1974. Deitanchi no chigaku (Geography of Peatland). University of Tokyo Press, Tokyo, pp. 329 (in Japanese).
Sakaguchi, Y., 1979. Distribution and genesis of Japanese peatlands. Bull. Dep. Geol., Univ. Tokyo 11, 17–42.
Shanahan, T.M., McKay, N.P., Hughen, K.A., Overpeck, J.T., Otto-Bliesner, B., Heil, C.W., King, J., Scholz, C.A., Peck, J., 2015. The time-transgressive termination of the African Humid Period. Nat. Geosci. 8, 140–144.
Slingerland, R., Smith, N.D., 2004. River avulsions and their deposits. Annu. Rev. Earth Planet. Sci. 32, 257–285.
Smith, N.D., Cross, T.A., Dufficy, J.P., Clough, S.R., 1989. Anatomy of an avulsion. Sedimentology 36, 1–23.
Smith, V.C., Staff, R.A., Blockley, S.P.E., Bronk Ramsey, C., Nakagawa, T., Mark, D.F., Takemura, K., Danhara, T., Suigetsu 2006 Project Members, 2013. Identification and correlation of visible tephras in the Lake Suigetsu SG06 sedimentary archive, Japan: chronostratigraphic markers for synchronising of east Asian/west Pacific palaeoclimate records across the last 150 ka. Quat. Sci. Rev. 67, 121–137.
Stott, L., Cannariato, K., Thunnell, R., Haug, G.H., Koutavas, A., Lund, S., 2004. Decline of surface temperature and salinity in the western tropical Pacific Ocean in the Holocene epoch. Nature 431, 56–59.
Stouthamer, E., Berendsen, H.J.A., 2001. Avulsion frequency, avulsion duration, and interavulsion period of Holocene channel belts in the Rhine-Meuse delta, the Netherlands. J. Sediment. Res. 71, 589–598.
Stouthamer, E., Berendsen, H.J.A., 2007. Avulsion: The relative roles of autogenic and allogenic processes. Sediment. Geol. 198, 309–325.
Tanabe, S., Saito, Y., Vu, Q.L., Hanebuth, T.J.J., Ngo, Q.L., Kitamura, A., 2006. Holocene evolution of the Song Hong (Red River) delta system, northern Vietnam. Sediment. Geol. 187, 29–61.
Thompson, D.M., Conroy, J.L., Collins, A., Hlohowskyj, S.R., Overpeck, J.T., Riedinger-Whitmore, M., Cole, J.E., Bush, M.B., Whitney, H., Corley, T.L., Kannan, M.S., 2017. Tropical Pacific climate variability over the last 6000 years as recorded in Bainbridge Crater Lake, Galápagos. Paleoceanography 32, 903–922.
Tian, Z., Li, T., Jiang, D., Chen, L., 2017. Causes of ENSO weakening during the mid-Holocene. J. Clim. 30, 7049–7070.
Tomita, K., 2010. Distribution, formation, and classification of wet grassland on mineral soils in Japan. Wetland Res. 1, 67–86 (in Japanese with English abstract).
Toonen, W.H.J., van Asselen, S., Stouthamer, E., Smith, N.D., 2016. Depositional development of the Muskeg Lake crevasse splay in the Cumberland Marshes (Canada). Earth Surf. Process. Landf. 41, 117–129.
Törnqvist, T.E., 1994. Middle and late Holocene avulsion history of the River Rhine (Rhine-Meuse delta, Netherlands). Geology 22, 711–714.
Tsukada, M., 1981. The last 12,000 years-the vegetation history of Japan II. New pollen zones. Jpn. J. Ecol. 31, 201–215 (in Japanese with English abstract).
Wanner, H., Beer, J., Bütikofer, J., Crowley, T.J., Cubasch, U., Flückiger, J., Goose, H., Grosjean, M., Joos, F., Kaplan, J.O., Küttel, M., Müller, S.A., Prentice, I.C., Solomina, O., Stocker, T.F., Tarasov, P., Wagner, M., Widmann, M., 2008. Mid- to Late Holocene climate change: an overview. Quat. Sci. Rev. 27, 1791–1828.
Wu, X., Zhang, Z., Xu, X., Shen, J., 2012. Asian summer monsoonal variations during the Holocene revealed by Huguangyan maar lake sediment record. Palaeogeogr. Palaeoclimatol. Palaeoecol. 323–325, 13–21.
Xiao, J., Si, B., Zhai, D., Itoh, S., Lomtatidze, Z., 2008. Hydrology of Dali Lake in central-eastern Inner Mongolia and Holocene East Asian monsoon variability. J. Paleolimnol. 40, 519–528.
Yabe, K., 1989. Comparative ecology of lowland mires: the comparison between the warm-temperate mires and the cool-temperate mires. Mem. Environ. Sci., Hokkaido University 4, 1–49 (in Japanese with English abstract).
Yasuda, Y., 1974. Palynology and archaeology since the last glacial age in Japan. Quat. Res. (*Daiyonki Kenkyuu*) 13, 106–134 (in Japanese with English abstract).
Yasuda, Y., 1978. Vegetational history and paleogeography of the Kawachi Plain for the last 13,000 years. Quat. Res. (*Daiyonki Kenkyuu*) 16, 211–229 (in Japanese with English abstract).
Yokoyama, Y., Okuno, J., Miyairi, Y., Obrochta, S., Demboya, N., Makino, Y., Kawahata, H., 2012. Holocene sea-level change and Antarctic melting history derived from geological observations and geophysical modeling along the Shimokita Peninsula, northern Japan. Geophys. Res. Lett. 39, L13502.
Yokoyama, Y., Maeda, Y., Okuno, J., Miyairi, Y., Kosuge, T., 2016. Holocene Antarctic melting and lithospheric uplift history of the southern Okinawa trough inferred from mid- to late-Holocene sea level in Iriomote Island, Ryukyu, Japan. Quat. Int. 397, 342–348.
Zhao, Y., Yu, Z., Chen, F., Zhang, J., Yang, B., 2009. Vegetation response to Holocene climate change in monsoon-influenced region of China. Earth Sci. Rev. 97, 242–256.
Zhao, C., Yu, Z., Zhao, Y., Ito, E., Kodama, K.P., Chen, F., 2010. Holocene millennial-scale climate variations documented by multiple lake-level proxies in sediment cores from Hurleg Lake, Northwest China. J. Paleolimnol. 44, 995–1008.
Zhu, Z., Feinberg, J.M., Xie, S., Bourne, M.D., Huang, C., Hu, C., Cheng, H., 2017. Holocene ENSO-related cyclic storms recorded by magnetic minerals in speleothems of central China. Proc. Natl. Acad. Sci. U. S. A. 114, 852–857.